Atomistic modeling of strain and diffusion at the Si/SiO_2 interface

Patrick Ganster, Guy Tréglia, and Andrés Saúl
Centre Interdisciplinaire de Nanoscience de Marseille, CNRS, Campus de Luminy, Case 913, 13288 Marseille Cedex 9, France
(Received 12 October 2009; revised manuscript received 24 December 2009; published 20 January 2010)

In this paper, we present a theoretical study of the elastic deformations arising in the vicinity of the Si/SiO_2 interface upon oxidation of a silicon substrate. The oxidation is modelized using an algorithm which alternates the inclusion of oxygen atoms and Molecular Dynamics simulations at high temperature. We find that the SiO_2 film undergoes an overall compressive state while a more complex strain field is found in the first few Si layers under the interface where tensile and compressive microstructures coexist, the former being definitely larger than the latter. The analysis of the formation energies of the main defects responsible for Si diffusion reveals that, in spite of the complexity of the deformation field at the Si/SiO_2 interface, their dependence with respect to the local deformation obeys the same laws as those derived from the application of a simple biaxial stress.

DOI: 10.1103/PhysRevB.81.045315 PACS number(s): 61.72.−y, 68.35.Gy, 61.43.Bn, 81.65.Mq

I. INTRODUCTION

Used as gate material in complementary metal-oxide semiconductor (CMOS) technology, silicon oxide was extensively studied in relation with the development of micro and nanoelectronics.[1–4] Of particular interest is the generation of an inhomogeneous strain field close to the silicon/oxide interface, which can have important consequences. For example, as the carrier mobility in Si is enhanced under strain,[5] it has been shown that the stress induced during oxidation can significantly increase the transconductance of a nanowire field-effect transistor (FET).[6] Controlling strain is then a challenge and its characterization both experimentally and theoretically an important advancement.[7,8] Indeed, with the continuous decrease in the size of devices, it becomes important to understand the properties of materials and boundaries at lower and lower dimensions, which requires to develop specific experimental and numerical methods. From the former point of view, recent methods like holography interferometry allow to map strain in materials at nanometric scale with high resolution.[9]

In this context, the goal of this paper is twofold. First, we will characterize the stress and deformations undergone by a silicon substrate under oxidation. Then, we will study how diffusion is modified under this strain field. To this aim, we model the formation of a silicon oxide grown on a silicon substrate using an algorithm which alternates the inclusion of oxygen atoms and atomic relaxations using Molecular Dynamics. The total energy and forces are calculate using a suited semiempirical potential developed a few years ago by Watanabe *et al.*[10] This procedure allows us to build a realistic Si/SiO_2 interface on both sides of which we characterize the structural deformations and calculate the stress field. Then, from the strain induced in the Si substrate, we calculate the formation energies of the two main defects (vacancy, dumbbell interstitial) responsible for diffusion of Si atoms. We show that, in spite of the complexity of the deformation field, their dependence with respect to local deformation obeys the same laws as those derived from the application of a simple biaxial stress.[11]

II. METHODOLOGY

A. Potential for Si/SiO_2 interface

The Stillinger-Weber (SW) potential,[12] originally developed to describe bulk silicon, is a widely used semiempirical potential composed of two-body and three-body terms, which was adapted to describe numerous multicomponent systems presenting diamondlike or amorphous structures. In addition, it has been shown recently that it was particularly suited to properly describe atomic diffusion in bulk Si.[11]

A few years ago, Watanabe *et al.* proposed a new parametrization and improvements of this SW potential to deal with Si/SiO_2 interfaces.[10,13,14] In this new version, which is still composed of a two-body part for SiSi, OO and SiO and three-body terms for SiSiSi, SiOSi, OSiO, and SiSiO, a bond order function g_{ij} has been added which modifies the two-body terms acting on the Si-O pairs.[10]

In this framework, the two-body term for a pair of atoms $i,j=\mathrm{Si},\mathrm{O}$ at a distance r_{ij} writes

$$V_{ij} = \epsilon g_{ij} A_{ij}\left[B_{ij}\left(\frac{\sigma}{r_{ij}}\right)^p - \left(\frac{\sigma}{r_{ij}}\right)^q\right]\exp\left(\frac{\sigma}{r_{ij}-D_{ij}}\right), \quad (1)$$

where

$$g_{ij} = \begin{cases} 1 & i=j \\ \dfrac{m_1}{\exp\left[\dfrac{m_2-z_i}{m_3}\right]+1}\exp[m_4(z_i-m_5)^2] & i\neq j \end{cases}, \quad (2)$$

with

$$z_i = \sum_k f_c(r_{ik}) \quad (3)$$

and

 ©2010 The American Physical Society

TABLE I. Two- and three-body parameters of the Stillinger-Weber potential used to describe the Si-O system.

ϵ (eV)	σ (Å)	r_1 (Å)	r_2 (Å)	m_1	m_2	m_3	m_4	m_5
2.1696	2.0951	1.20	1.40	0.097	1.6	0.3654	0.1344	6.4176

$i-j$	p_{ij}	q_{ij}	A_{ij}	B_{ij}	D_{ij}
Si-Si	4.0	0	7.049556277	0.6022245584	1.80
Si-O	2.58759	2.39370	115.364065913	0.9094442793	1.40
O-O	0	2.24432	−12.292427744	0	1.25

$j-i-k$	λ_{jik}	γ_{jik}^{ij}	γ_{jik}^{ik}	a_{jik}^{ij}	a_{jik}^{ik}	$\cos\,\theta_{jik}^{0}$
Si-Si-Si	21.0	1.2	1.2	1.80	1.80	−1/3
Si-Si-O	10.667	1.93973	0.25	1.90	1.40	−1/3
O-Si-O	3.1892	0.3220	0.3220	1.65	1.65	−1/3
Si-O-Si	2.9572	0.71773	0.71773	1.40	1.40	−0.6155238

$$f_c(r) = \begin{cases} 1 & r < r_1 \\ 1 - \dfrac{r-r_1}{r_2-r_1} + \dfrac{1}{2\pi}\sin\left[\dfrac{2\pi(r-r_1)}{r_2-r_1}\right] & r_1 \le r < r_2 \\ 0 & r \ge r_2 \end{cases}, \quad (4)$$

a cut-off function. The three-body terms write

$$V_{jik} = \epsilon\lambda_{jik}\exp\left[\frac{\gamma_{jik}^{ij}\sigma}{r_{ij}-a_{jik}^{ij}\sigma} + \frac{\gamma_{jik}^{ik}\sigma}{r_{ik}-a_{jik}^{ik}\sigma}\right](\cos\,\theta_{jik} - \cos\,\theta_{jik}^{0})^2. \quad (5)$$

The parametrization of both terms was established from experimental data and *ab initio* calculations of structural and energetic properties of silica phases. The numerical values for all the parameters that were used in this work are summarized in Table I. They are exactly the same as the ones proposed by Watanabe *et al.* except for λ_{SiSiSi} for which we have used the original Stillinger-Weber parametrization, $\lambda_{SiSiSi}=21.0\epsilon$ instead of 16.404ϵ. The reason for doing that was to facilitate the comparison with the numerous studies realized in pure silicon with the original SW potential, in particular concerning the point defect energies in the silicon substrate.[11] We have checked that this modification does not change significantly the structures and morphologies of bulk SiO_2 and the SiO_2/Si interface.

B. Stress tensor calculation

An instantaneous total stress tensor can be defined as follows:

$$\sigma_{\alpha\beta} = \frac{1}{\Omega}\frac{\partial E}{\partial \epsilon_{\alpha\beta}}, \quad (6)$$

where E is the total energy of N atoms in a volume Ω and $\epsilon_{\alpha\beta}$ is a component of the strain tensor ($\alpha,\beta = x, y$, or z). The total energy E being a function of the momentum and the position vectors of atoms, the tensor $\sigma_{\alpha\beta}$ can be decomposed as the sum of a kinetic and a potential contribution

$$\sigma_{\alpha\beta} = \sigma_{\alpha\beta}^{kin} + \sigma_{\alpha\beta}^{pot} = -\frac{1}{\Omega}\sum_{i=1}^{N}\frac{p_i^{\alpha}p_i^{\beta}}{m_i} + \frac{1}{\Omega}\sum_{i=1}^{N} r_i^{\beta}\frac{dV}{dr_i^{\alpha}}, \quad (7)$$

where V is the potential energy, and p_i and r_i are the momentum and position vectors of the ith atom with mass m_i. In the particular case of the Stillinger-Weber potential, the second term of the instantaneous stress tensor also contains two-body and three-body components

$$\sigma_{\alpha\beta}^{pot} = \sigma_{\alpha\beta}^{2b} + \sigma_{\alpha\beta}^{3b} = \frac{1}{\Omega}\sum_{i=1}^{N}[\sigma_{\alpha\beta}^{2b}(i) + \sigma_{\alpha\beta}^{3b}(i)], \quad (8)$$

where $\sigma_{\alpha\beta}^{2b}(i)$ and $\sigma_{\alpha\beta}^{3b}(i)$ are the contributions of atom i to the respective potential parts of the stress tensor. They can be written as

$$\sigma_{\alpha\beta}^{2b}(i) = \frac{1}{2\Omega}\sum_{j\neq i}\frac{1}{r_{ij}}\frac{\partial V_{ij}}{\partial r_{ij}}R_{ij}^{\alpha}R_{ij}^{\beta} \quad (9)$$

and

$$\sigma_{\alpha\beta}^{3b}(i) = \frac{1}{2\Omega}\sum_{j\neq i}\sum_{k\neq i\neq j}\left[\frac{1}{r_{ij}}\frac{\partial V_{jik}}{\partial r_{ij}}R_{ij}^{\alpha}R_{ij}^{\beta} + \frac{1}{r_{ik}}\frac{\partial V_{jik}}{\partial r_{ik}}R_{ik}^{\alpha}R_{ik}^{\beta} + \frac{1}{r_{jk}}\frac{\partial V_{jik}}{\partial r_{jk}}R_{jk}^{\alpha}R_{jk}^{\beta}\right], \quad (10)$$

where r_{ij}, r_{ik}, r_{jk} are the interatomic distances for atomic pairs ij, ik and jk and R_{ij}^{α} the component α of the vector difference $\vec{R}_{ij} = \vec{r}_i - \vec{r}_j$. The Eqs. (8)–(10) allow us to calculate the atomic contributions of the stress tensor. These definitions are used in the following to describe stress at the atomic level.

C. Modeling the Si/SiO_2 interface: Oxidation of a silicon substrate

The modelization of the silicon oxidation is performed following a methodology originally proposed by Dalla Torre *et al.*[15] The initial configuration consists in a bare silicon substrate oriented in such a way as the x, y, and z axis of the simulation box are aligned along the [100], [010], and [001] directions of the diamond structure. The oxygen atoms being introduced along the z direction, no periodic boundary condition (PBC) is applied in the [001] direction, so that the system is free to relax in that direction. In order to avoid border effects on the edges of the simulation box, it is tempting to apply PBC in the [100] and [010] (x,y) directions. However, this may introduce artificial lateral strains in the SiO_2 oxide which will be only partially released by the vertical relaxation. In order to understand the relative importance of these assumptions, we have considered in this work two kinds of systems: the first one (labeled PBC) with periodic conditions in the x and y directions, and the second one (labeled NPBC) in which these periodic conditions are removed. They represent two ideal limiting cases, the PBC one corresponding to a system where no lateral relaxation is allowed and the NPBC where the system is totally free to relax. The former has an evident experimental counterpart corresponding to the oxidation of a Si substrate embedded in a stiff matrix while the second case would correspond to the oxidation of a mesa or crystalline dot under directional oxygen flux or embedded in a soft matrix.

A few oxygen atoms are initially located randomly at some Si dangling bonds on the Si(001) surface, which play the role of nuclei for oxidation. The numerical oxidation protocol consists in the inclusion of an oxygen atom every one thousand Molecular Dynamics steps. The inclusion step is performed as follows: we localize the highest Si atom which is bound to at least one and at most three oxygen atoms, we then search the longest Si–Si bond formed by the selected Si atom with its first neighbors, and we insert the oxygen atom randomly in the mediator plane of this bond, in such a way that the Si-O distances are 1.6 Å under the condition that there is no other oxygen atom in the neighboring (R_c $=2$ Å). For the Molecular Dynamics simulations, we use a time step for the integration of the equation of motion of 2 fs. The temperature is maintained at 1200 K applying a Maxwell-Boltzmann velocity distribution on the atomic system every one hundred time steps. For each system, the oxidation procedure is achieved over ~ 10 Si layers. In the case of the PBC systems, the box length in the x and y directions is scaled to the equilibrium parameter (zero external pressure) of the silicon substrate at 1200 K using the thermal expansion parameter of silicon $\alpha = 3.45 \times 10^{-6}$ K^{-1}, which has been previously determined by a constant pressure run in a pure silicon system of 512 atoms.[11] Once this procedure is finished, in order to calculate the formation energies of point defects the system is quenched to 0 K by constrained molecular dynamics and the box lengths are rescaled to the equilibrium parameter of silicon at 0 K. The reason for doing that is to compare with the 0 K formation energies calculated in our previous work (see below).[11]

We have considered simulation boxes with three different sizes: $3\times3\times12$, $5\times5\times10$, and $9\times9\times12$ unit cells (the unit cell is the nonprimitive diamond unit cell containing eight atoms). As the comparison between these systems have not evidenced any dependence with the box size, we will only present here the results obtained for the biggest cell having 162 Si atoms per (001) plane (a box length in the x and y directions of 48.88 Å) and containing 7776 Si atoms and 2819 O atoms.

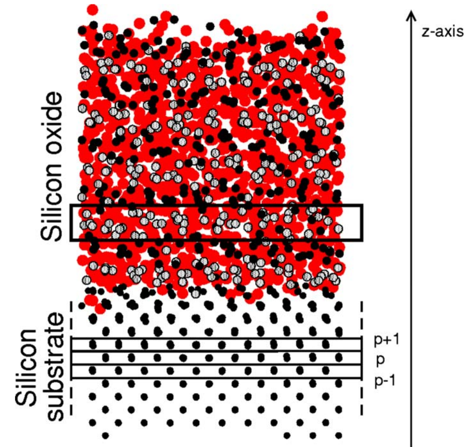

FIG. 1. (Color online) Schematic representation of the SiO_2/Si interface. Analysis is realized in slabs where thickness is defined with mass centers of silicon layers (001).

III. PROPERTIES OF THE SiO_2/Si SYSTEM

Due to our oxidation scheme, the oxide grows layer by layer through successive (001) oxidized silicon planes. This is illustrated in Fig. 1, in which the stacking of the oxidized silicon planes is represented in alternate colors (black/gray) in the silicon oxide. To make easier the structural and stress analysis of the system, we define generalized thick layers (hereafter referred to as *slabs*) both in the oxide and in the Si substrate in the following way. Before the oxygen insertion, the positions of the Si atoms belonging to a given (001) layer are collected, which allows to determine the mass center position of this layer all along the simulation. From the knowledge of the mass center positions of the silicon planes $p-1$, p, and $p+1$ in the z direction (see Fig. 1), a slab p of thickness δz^p is defined by $\delta z^p = \frac{1}{2}(z_{MC}^{p+1} - z_{MC}^{p}) - \frac{1}{2}(z_{MC}^{p} - z_{MC}^{p-1})$, where z_{MC}^{p} is the z coordinate of the mass center of the pth (001) silicon plane.

The projections of the atomic positions in xz plane of the SiO_2/Si system at a given state of oxidation are shown in Fig. 2(a). The silicon substrate (nonoxidized silicon) extends from 0 to 50 Å in the z axis while the oxide silicon occupies the region from 50 to 80 Å.

A. Structural analysis

The structural analysis of the silicon oxide grown by our oxidation procedure is detailed here in the case of PBC systems, since the presence or the absence of periodic boundary conditions do not affect the general features. The essential result is that this oxide can be viewed as an amorphous SiO_2

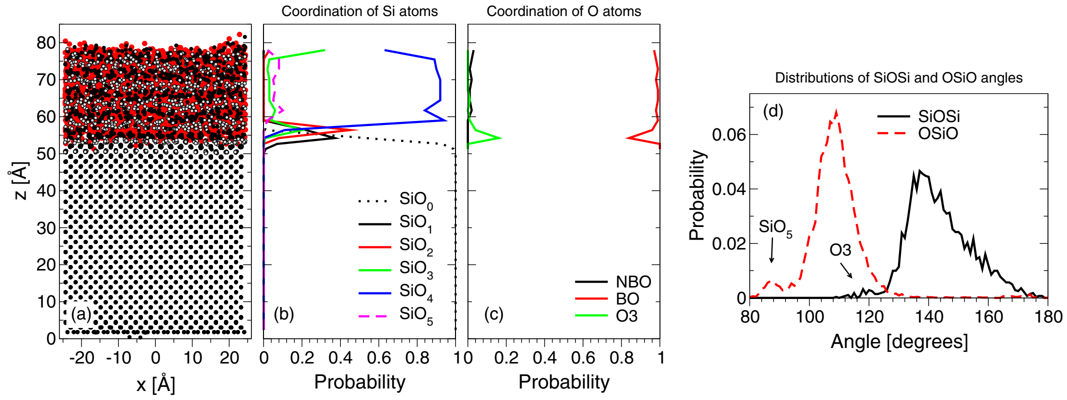

FIG. 2. (Color online) The atomic system is recalled in (a) as a guide for the eyes. The coordinations of Si atoms and O atoms are plotted as a function of z, in (b) and (c), respectively. The distributions of the OSiO and SiOSi angles calculated in the oxide are shown in (d).

compound, mainly composed of SiO_4 tetrahedra linked by bridging oxygen (BO).

The coordination of Si and O atoms has been calculated using a cutoff radius of 2.0 Å, consistently with the distribution of SiO distances, which vanishes at 2.0 Å after a first maximum centered around 1.62 Å. Their dependence as a function of z is displayed in Figs. 2(b) and 2(c) for Si and O, respectively. As can be seen in Fig. 2(b), the silicon oxide is composed of about 90% of fourfold coordinated Si. The other Si atoms present in general a lower coordination, except for the fivefold ones, which only exist in the middle of the oxide layer, avoiding both the SiO_2 surface and interface. The presence of such entities, which are commonly observed in amorphous silica under high pressure,[16,17] are related to the compression induced by the oxidation procedure, which is particularly important when applying periodic boundary conditions (see next section). On the contrary, the few threefold coordinated Si present in the structure are essentially found in the vicinity of the SiO_2 surface and interface. The existence of such entities at the surface of the SiO_2 oxide has already been mentioned in other structural models of amorphous silica surfaces.[18,19] Finally, all the less coordinated Si atoms can be found in the interfacial region, which can be viewed as the transient region between a crystalline to an amorphous structure, in good agreement with photoemission results[20] which also reveal the presence of SiO_1 and SiO_2 species.

Details on the nature of the oxygen bonding are given in Fig. 2(c), which shows the probability of finding bridging oxygens (BO, oxygen linked to two silicon atoms), nonbridging oxygens (NBO, oxygen linked to one silicon atom) and tricluster oxygens (O3, oxygen linked to three silicon atoms) in the sample. In the middle of the silicon oxide, the atoms are practically all bridging atoms, even though one can also find a few NBO ones. A very slight increase in the number NBO atoms can be observed at the SiO_2 surface. A more important effect is the increase in the O3 species in the vicinity of the SiO_2/Si interface. These overcoordinated atoms only exist in this region and disappear far from the oxidation front.

In order to determine to what extent the grown oxide can be considered as amorphous, one can either calculate the pair correlation function or the SiOSi and OSiO angle distributions. The former has not been done here due to problems in defining an actual normalization for the correlation function in presence of a free surface. Therefore, only the angular distribution has been used, which is sufficient to conclude whether the structure is amorphous or not. In Fig. 2(d), we show the distribution of the OSiO and SiOSi angles in the oxide region. The mean value of the OSiO one is about 109° corresponding to the tetrahedron environment of silicon, and that of the SiOSi angle is about 145°. As shown by the arrows the small bumps around 90° and 120° correspond, respectively, to the fivefold coordinated silicon atoms and the threefold coordinated oxygen atoms. The overall spread of the angle distributions confirms the amorphous character of the SiO_2 oxide.

B. Stress profile

Let us now analyze the stress profile induced by oxidation both in the growing oxide and in the silicon substrate. As previously stated, the study is realized both on the constrained PBC system (periodic boundary conditions applied in the x and y directions) and in the relaxed NPBC one (no periodic boundary conditions). Using the notations of the instantaneous stress tensor defined in Sec. II B, we can decompose the stress profile along the z direction into its contributions $\sigma^p_{\alpha\beta}$ within the slabs (labeled p) defined in Sec. III A as follows:

$$\sigma^p_{\alpha\beta} = \sum_{i=1}^{n} [\sigma^{kin}_{\alpha\beta}(i) + \sigma^{2b}_{\alpha\beta}(i) + \sigma^{3b}_{\alpha\beta}(i)], \quad (11)$$

where n is the number of atoms in the slab p of volume $\Omega = \delta z^i \times L_x \times L_y$, $\sigma^{\alpha\beta}_{kin}(i)$, $\sigma^{2b}_{\alpha\beta}(i)$, and $\sigma^{3b}_{\alpha\beta}(i)$ are defined in Eqs. (9) and (10), respectively.

The Fig. 3(b) shows the stress profiles calculated at 0 K for the system with periodic boundary condition [the atomic structure is shown in Fig. 3(a)]. We present the profiles for the components σ_{xx}, σ_{yy}, σ_{zz}, and the pressure defined as $P = -\frac{1}{3}Tr(\sigma)$. One can see that, since the system is fully relaxed in the z direction, $\int \sigma_{zz} dz = 0$, which is obviously not the case for σ_{xx} and σ_{yy}. The silicon oxide is found in a very compressive state in both x and y directions. Indeed, in spite of partial relaxation in the z direction, a strong compressive

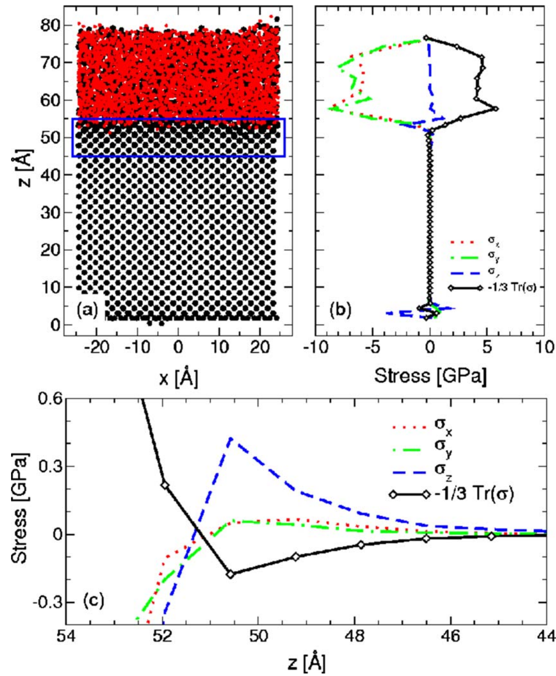

FIG. 3. (Color online) PBC system: (a) atomic configuration quenched to 0 K after thermal equilibration at 1200 K, (b) corresponding profile of the stress components σ_{xx}, σ_{yy}, σ_{zz}, and $-\frac{1}{3}Tr(\sigma)$ in the whole system, and (c) in the rectangular region close to the SiO_2/Si interface shown in (a).

stress remains after equilibration due to the periodic boundary condition. This leads to a mass density on the order of 2.6 g cm^{-3}, which is slightly higher than the experimental[21,22] of about 2.3 g cm^{-3}. In the vicinity of the SiO_2/Si interface, the silicon substrate undergoes a tensile stress [see inset of Fig. 3(b)]. This stress is two orders of magnitude lower than the stress observed in the silicon oxide and vanishes beyond five silicon planes. This differs from the results of Dalla Torre *et al.*,[15] who observed a compressive stress in the vicinity of the SiO_2/Si interface. We do not know what the actual origin of this discrepancy is, it can be a consequence of their slab definition or to the use of instantaneous instead of average values. We have verified that it is not due to our procedure consisting of quenching and rescaling the lattice parameters since we obtain similar stress profiles at 1200 K. On the nonoxidized silicon surface (bottom silicon layers), silicon reconstruction occurs leading to a complex stress profile.

Let us now present in Fig. 4 the equivalent stress profiles for the NPBC system. The main effect of removing the periodic boundary conditions in the *x* and *y* directions is on the one hand to strongly decrease the compressive stress in the oxide and on the other hand to enhance the tensile stress region in the silicon substrate which now vanishes only beyond 10–12 Å. Indeed, in the absence of PBC in the *x* and *y* directions, the σ_{xx} and σ_{yy} components now also verify $\int\sigma_{xx}dx=\int\sigma_{yy}dy=0$, which implies that the stress in the oxide is compensated by the stress in the silicon substrate. In the middle of the oxide (z coordinate around 65 Å) the *xx* and *yy* stress components are almost zero. The size of this fully relaxed region increases if one continues the oxidation process while the tensile and compressive zones concentrate near the surface and the Si/SiO_2 interface. Close to the interface, the mean value of the compressive stress in the oxide (~0.5 GPA) is in good agreement with experimental measurements.[23]

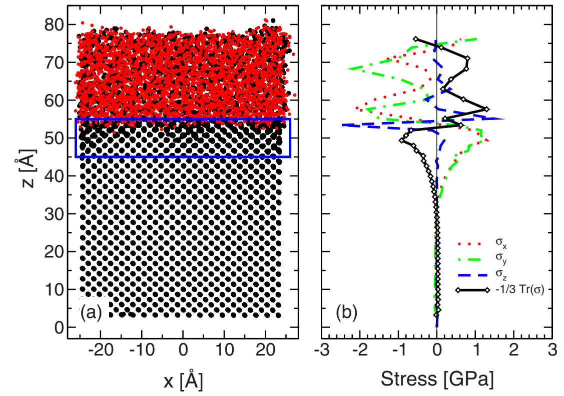

FIG. 4. (Color online) NPBC system: (a) atomic configuration quenched to 0 K after thermal equilibration at 1200 K and (b) corresponding profile of the stress components σ_{xx}, σ_{yy}, σ_{zz}, and $-Tr(\sigma)$.

The influence of the periodic boundary conditions in the *x* and *y* directions can be still better visualized in Fig. 5 in which the stress component profiles are presented separately. As can be seen, in the PBC system, the tensile stress in the silicon substrate is mainly due to the σ_{zz} component, which is damped beyond five silicon planes from the interface, the contribution of the σ_{xx} and σ_{yy} components is very weak and vanishes beyond three layers. On the contrary, in the NPBC system, the contribution of the σ_{zz} component becomes negligible, the tensile stress in the silicon substrate being now due to the σ_{xx} and σ_{yy} components. This means that the substrate can be viewed as supporting an anisotropical biaxial stress in this case. The tensile stress in the silicon substrate now extends farther and disappears within 14–15 silicon layers (~20 Å).

IV. FORMATION OF DEFECTS IN THE VICINITY OF THE SiO_2/Si INTERFACE

The formation energy of point defects is an essential quantity entering in the evaluation of the self-diffusion coefficient. Furthermore, its relative dependence with the local deformation can modify the nature of the mechanism which mediates the diffusion. In order to study this problem, we will characterize here the local deformations in the silicon substrate, and then evaluate the formation energy of the most usual point defects (vacancy and interstitial) in the silicon layers close to the SiO_2/Si interface.

To evaluate the local deformation $\underline{\epsilon}$ in the silicon substrate we define tetrahedron volumes V_t for each silicon atom and their four neighbors. From the tetrahedron volume defined in the perfect crystal V_0, we estimate the local strain from the tetrahedron volume variation $\delta V=V_t-V_0$, which depends on the nature of the deformation considered, i.e., for a biaxial strain $\epsilon_{\parallel}$

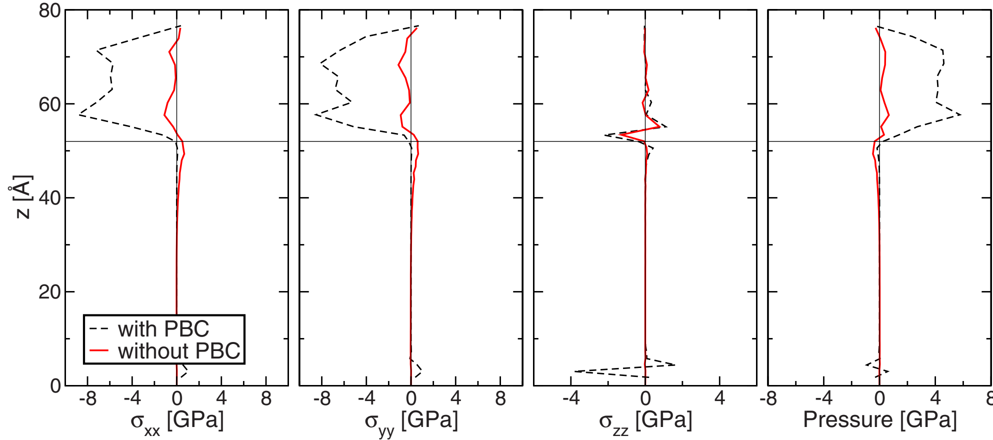

FIG. 5. (Color online) Comparison of the stress component profiles with and without applying PBC. The horizontal line corresponds to the position of the lower oxygen in the oxide.

$$\delta V/V_0 = 2\epsilon_{\parallel}\left[\frac{2\nu-1}{\nu-1}\right], \qquad (12)$$

where ν is the Poisson coefficient.

In Figs. 6(a) and 6(b), we show maps of the local deformation in the most tensile silicon plane close to the interface for the PBC and NPBC systems, respectively. In both cases, these maps reveal that, in spite of an average tensile stress, compressive areas also exist, the deformation fluctuating from −2.5% (compressive strain) to +2.5% (tensile strain). In the PBC system, the size of the compressive domains is on the order of that of tensile domains (~10 Å), resulting in a very weak global stress. In the NPBC system, the compressive domains are smaller, which explains that the average stress in the layer is now significantly tensile.

For each site in the interface silicon layer, we calculate the formation energy of the main defects responsible for Si self-diffusion (vacancies, extended dumbbell interstitial).[11] To study the local formation energy of a vacancy at a given site, we remove the corresponding silicon atom, and then we quench the full system using a constrained Molecular Dynamics algorithm. The local vacancy formation energy ΔE_f^{V} is calculated as the energy involved when one atom is removed from the given site and placed in a *reservoir*

$$\Delta E_f^{\mathrm{V}} = E^{\mathrm{V}}_{\mathrm{SiO_2/Si}} + E^{c}_{\mathrm{Si}} - E_{\mathrm{SiO_2/Si}}, \qquad (13)$$

where $E^{\mathrm{V}}_{\mathrm{SiO_2/Si}}$ is the energy of the quenched system with a vacancy, E^{c}_{Si} is the cohesive energy of a nonconstrained silicon system (*reservoir*), and $E_{\mathrm{SiO_2/Si}}$ is the energy of the SiO_2/Si system before removing the silicon atom. The corresponding results as a function of the local deformation $\delta V/V_0$ (before introduction of the defect) are shown in Fig. 6(c) for the PBC system and in Fig. 6(d) for the NPBC one. In the latter case, we have separated the sites belonging to the inner (physical) region of the layer (black square dots) from those belonging to the border (gray crosses).

As can be seen, in spite of some dispersion, the vacancy formation energy appears to be well correlated with the local deformation. The dependence of the mean value of the distribution is quasilinear, with a similar slope for both the PBC and NPBC systems. Since the Si substrate undergoes an anisotropic biaxial stress, it is tempting to see to what extent the present local dependence can be related to the equivalent dependence of an homogeneous biaxial strain. We have studied the latter case in a previous paper[11] where we have used the same SW potential and a cubic system containing 512 silicon atoms to calculate the defect formation energies of a constrained film with a free surface. We have found that for vacancies the overall effect of a positive biaxial strain is to increase the formation energy (see details in Ref. 11). This is quite natural since the creation of a vacancy locally induces a tensile stress which is further increased (reduced) under dilation (compression). The consequence is that it is easier to create a vacancy in a compressed lattice.

The corresponding curve is presented in Figs. 6(c) and 6(d) as a green solid line where we have used Eq. (12) with $\nu \sim \frac{1}{3}$ to transform the biaxial strain used in Ref. 11 to the volume deformation used in this work ($\delta V/V_0 = \epsilon_{\parallel}$). As can be seen it almost perfectly interpolate between the dots, confirming the generality of the observed behavior.

In a similar way, we have calculated the formation energy of extended dumbbell interstitials (which are the stablest interstitials with the SW potential)[11]

$$\Delta E_f^{\mathrm{I}} = E^{\mathrm{I}}_{\mathrm{SiO_2/Si}} - E^{c}_{\mathrm{Si}} - E_{\mathrm{SiO_2/Si}}, \qquad (14)$$

where $E^{\mathrm{I}}_{\mathrm{SiO_2/Si}}$ is the energy of the quenched system with an interstitial. The corresponding interstitial formation energies are shown in Fig. 6(e) for the PBC system and in Fig. 6(f) for the NPBC one. As for vacancies, the formation energy is strongly dependent of the strain before insertion of the point defect, but the overall behavior is the inverse: the more tensile is the stress, the lower is the formation energy. We have also reported here the curves taken from Fig. 6(a) of Ref. 11 giving the formation energies for the two possible orientations of the extended dumbbell as a function of an isotropical biaxial strain. The red solid lines in Figs. 6(e) and 6(f) correspond to the ⟨110⟩ extended dumbbell oriented along the (110) plane and the blue dotted lines for the same defect oriented along the (101) one. As can be seen, the two lines still satisfactorily interpolate between the dots.

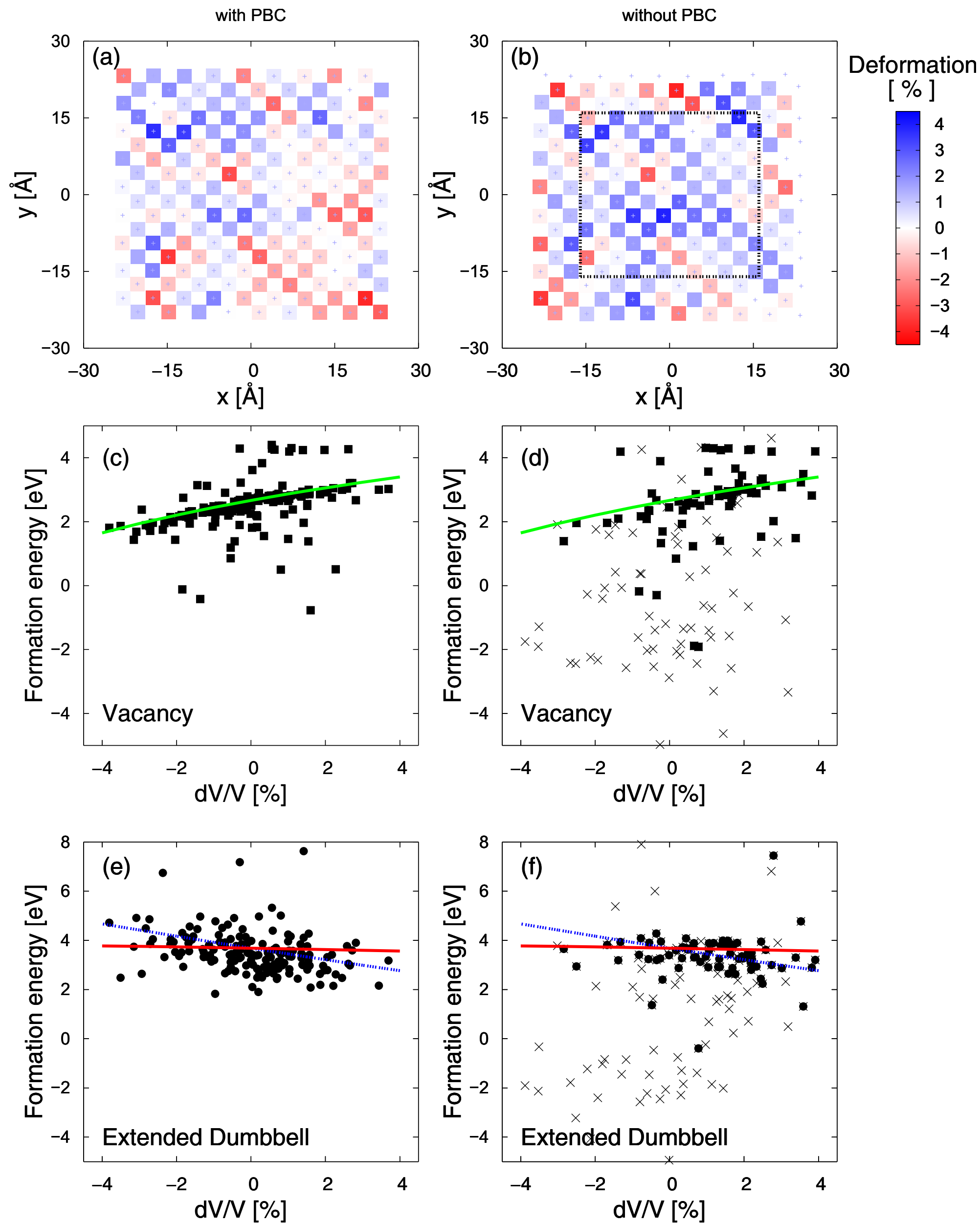

FIG. 6. (Color online) Schematic representation of the strain field at the SiO_2/Si interface for (a) a system with periodic boundary conditions PBC and (b) a system without PBC. The dependence between the vacancy formation energies and the local deformation for the PBC system is shown in (c) and for the NPBC in (d). The dependence between the energy formation for extended dumbbells is shown in (e) for the PBC system and in (f) for the NPBC one. In the case of the NPBC system, the black circular dots correspond to sites belonging to the region of the layer delimited by a square in (b) and the red square dots to those outside. The green solid lines in (c) and (d) represent the dependence of the vacancy formation energy in the case of an isotropical biaxial strain. The red solid and blue dotted lines in (e) and (f) correspond, respectively, to the formation energies of the ⟨110⟩ extended dumbbell oriented along the (110) and (101) planes. They are all taken from Fig. 6(a) of Ref. 11.

V. CONCLUSIONS

In order to simulate silicon oxidation, we have used an algorithm which alternates the inclusion of oxygen atoms in a silicon substrate and Molecular Dynamics relaxations at high temperature. In the vicinity of the Si/SiO_2 interface, oxidation leads to a strain which drastically modifies the self-diffusion mechanisms in the Si substrate. Indeed, our main result is that the so-grown SiO_2 film undergoes an overall compressive state, a more complex strain field being found in the first few Si layers under the interface. In the latter case, tensile and compressive microstructures coexist, the former being definitely larger than the latter. The analysis of the formation energies of the main defects responsible for Si diffusion reveals that, in spite of the complexity of the deformation field at the Si/SiO_2 interface, their dependence

with respect to local deformation is similar to the one obtained from the application of an homogeneous biaxial stress.[11] This means that the general (T, ϵ) diagram derived in that case could be applied in the vicinity of a realistic SiO_2/Si interface to predict the leading diffusion mechanisms as a function of temperature (T) and local deformation ϵ.

ACKNOWLEDGMENTS

This work was founded by the French National Agency ANR through OSiGeSim Project No. ANR-05-NANO-004. We thank all the partners of this consortium for enlightening discussions.

[1] L. C. Feldman, E. P. Gusev, and E. Garfunkel, in *Fundamental Aspects of Ultrathin Dielectrics on Si-Based Devices*, edited by E. Garfunkel, E. P. Gusev, and A. Vul (Kluwer, Dordrecht, 1998), p. 124.

[2] D. J. Dumin, in *Oxide Reliability: A Summary of Silicon Oxide Wearout, Breakdown, and Reliability*, edited by D. J. Dumin (Clemson University, USA, 2002).

[3] A. Pasquarello, M. Hybertsen, and R. Car, Nature (London) **396**, 58 (1998).

[4] M. Itsumi, SiO_2 *in Si Microdevices* (Kodansha, Tokyo/Springer, Berlin, 2003).

[5] M. Lee, E. Fitzgerald, M. Bulsara, M. Currie, and A. Lochtefeld, J. Appl. Phys. **97**, 011101 (2005).

[6] A. Seike, T. Tange, I. Sano, Y. Sugiura, D. Kosemura, A. Ogura, and I. Ohdomari, Appl. Phys. Lett. **91**, 062108 (2007).

[7] P. Mooney, Mater. Sci. Eng., B **134**, 133 (2006).

[8] M. V. Fischetti, F. Gamiz, and W. Hansch, J. Appl. Phys. **92**, 7320 (2002).

[9] M. Hytch, F. Houdelier, F. Hue, and E. Snoeck, Nature (London) **453**, 1086 (2008).

[10] T. Watanabe, H. Fujiwara, H. Noguchi, T. Hoshino, and I. Ohdomari, Jpn. J. Appl. Phys. **38**, L366 (1999).

[11] P. Ganster, G. Tréglia, and A. Saúl, Phys. Rev. B **79**, 115205 (2009).

[12] F. H. Stillinger and T. A. Weber, Phys. Rev. B **31**, 5262 (1985).

[13] T. Watanabe and I. Ohdomari, Thin Solid Films **343-344**, 370 (1999).

[14] T. Watanabe, K. Tatsumura, and I. Ohdomari, Appl. Surf. Sci. **237**, 125 (2004).

[15] J. Dalla Torre, J.-L. Bocquet, Y. Limoge, J.-P. Crocombette, E. Adam, G. Martin, T. Baron, P. Rivallin, and P. Mur, J. Appl. Phys. **92**, 1084 (2002).

[16] J. Badro, D. M. Teter, R. T. Downs, P. Gillet, R. J. Hemley, and J. L. Barrat, Phys. Rev. B **56**, 5797 (1997).

[17] J. Horbach, J. Phys.: Condens. Matter **20**, 244118 (2008).

[18] M. Rarivomanantsoa, P. Jung, and R. Jullien, J. Phys.: Condens. Matter **13**, 6707 (2001).

[19] B. Feuston and S. Garofalini, J. Chem. Phys. **91**, 564 (1989).

[20] J. H. Oh, H. W. Yeom, Y. Hagimoto, K. Ono, M. Oshima, N. Hirashita, M. Nywa, A. Toriumi, and A. Kakizaki, Phys. Rev. B **63**, 205310 (2001).

[21] N. Awaji, S. Ohkubo, T. Nakanishi, Y. Sugita, K. Takasaki, and S. Komiya, Jpn. J. Appl. Phys. **35**, L67 (1996).

[22] S. Kosowsky, S. Pershan, K. Krisch, J. Bevk, M. Green, L. Feldman, and P. Roy, Appl. Phys. Lett. **70**, 3119 (1997).

[23] P. Donnadieu, E. Blanquet, N. Jakse, and P. Mur, Appl. Phys. Lett. **85**, 5574 (2004).